Special Collection

# A Study on Varying the Number of Fluorene Units in 2, 1, 3-Benzothiadiazole-Containing Oligomers and the Effect on OLED Performance and Stability

Luis-Abraham Lozano-Hernández,[a, b] Joseph Cameron,*[a] Christopher J. Riggs,[a] Sebastian Reineke,[c] and Peter J. Skabara*[a]

Solution-processing has the potential to reduce the cost and energy requirements in the fabrication of organic light-emitting diode (OLED) devices. In non-doped emissive layers, polymers are commonly used but often suffer from batch-to-batch variation. Oligomers, which have precise molecular structures, avoid this problem but maintain the favourable film-forming properties that polymers possess. We present three benzothiadiazole-containing fluorene-based oligomers, **BT-F3$_2$**, **BT-F4$_2$** and **BT-F5$_2$**, which have terfluorene, quaterfluorene and pentafluorene arms, respectively, attached to a benzothiadiazole core. The materials show very high photoluminescence quantum yields, with **BT-F4$_2$** exhibiting the highest PLQY of 0.96 in the thin film. Although there is little change in the electroluminescence spectra, the oligomer size influences device performance. **BT-F3$_2$** had an external quantum efficiency of 1.9% and high luminance whilst **BT-F4$_2$** reached an external quantum efficiency of 2.3%. Furthermore, the stability of the OLED devices was evaluated and showed that the device lifetime decays with increasing molecular length.

## Introduction

Organic light-emitting diodes (OLEDs) have attracted considerable attention due to their attractive properties such as low power consumption, fast response, flexibility and high contrast.[1] Additionally, the ability to create OLEDs using solution-processing methods means these devices have the potential to be lower cost with reduced energy intensive fabrication required, compared to vacuum deposition, using methods such as inkjet printing, screen printing or slot-die coating.[2]

It remains a challenge to develop emissive materials that are suitable for solution-processing but also exhibit high efficiency, high luminance and long device lifetime when used in OLEDs, properties that are necessary for a wide variety of applications. Polymer emissive materials have advantages such as good solubility and processability for wet techniques, scalability and good mechanical properties.[3] However, polymers suffer from batch-to-batch variation which can in turn affect the reproducibility of OLEDs using polymer emissive layers (EMLs). On the other hand, small molecules and oligomers possess absolute synthetic reproducibility, monodispersity, and can maintain the favourable film-forming properties using solution-processing methods that polymers also show,[4] making such materials ideal for use in place of polymer emissive materials.

Due to these advantages, we have studied three 2,1,3-benzothiadiazole-containing oligofluorene emissive materials (Figure 1) which are highly luminescent. The three materials **BT-F3$_2$**, **BT-F4$_2$** and **BT-F5$_2$** contain a 2,1,3-benzothiadiazole (BT) core, capped with ter-, quater- and pentafluorene arms, respectively, attached at the 4- and 7- positions. BT is a popular electron deficient unit that has been used in active materials for optoelectronic applications such as OLED[5] and organic

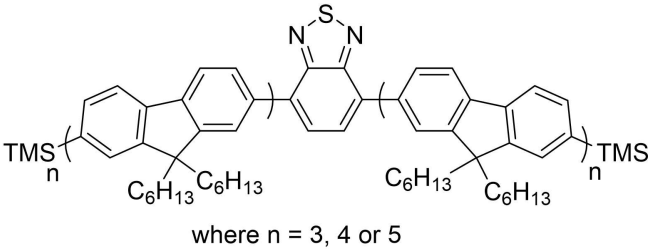


**Figure 1.** The structures of **BT-F3$_2$**, **BT-F4$_2$** and **BT-F5$_2$**.

[a] Dr. L.-A. Lozano-Hernández, Dr. J. Cameron, C. J. Riggs, Prof. Dr. P. J. Skabara
WestCHEM, University of Glasgow
Joseph Black Building, School of Chemistry
University Avenue, G12 8QQ Glasgow (UK)
E-mail: Joseph.Cameron@glasgow.ac.uk
peter.skabara@glasgow.ac.uk
[b] Dr. L.-A. Lozano-Hernández
Research Group of Optical Properties of Materials (GPOM)
Centro de Investigaciones en Óptica A.P. 1-948
C.P. 37000 León, Guanajuato (México)
[c] Prof. Dr. S. Reineke
Technische Universität Dresden
Dresden Integrated Center for Applied Physics and Photonic Materials (IAPP)
Nöthnitzer Str. 61, 01187 Dresden (Germany)

Supporting information for this article is available on the WWW under https://doi.org/10.1002/cptc.202200256

An invited contribution to a Special Collection on Emissive Materials for Organic Light Emitting Diodes

photovoltaic devices,[6] and for gain materials for amplified spontaneous emission.[7] Typically, the electron deficient nature of BT causes localisation of the lowest unoccupied molecular orbital (LUMO) and a reduction in energy *vs* vacuum and this can lower the electron injection barrier for the emissive layer of an OLED for example.[8]

One of the most popularly used BT-containing materials for OLEDs is the polymer F8BT which was first developed by The Dow Chemical Company in 1998.[9] It has shown promising performance in OLED emissive layers. For example, Lee and co-workers reported inverted polymer OLEDs with an emissive layer of 1200 nm showing an external quantum efficiency of 17.8%.[10] Therefore, it is important to develop oligomer analogues of polymers such as F8BT, to attempt to maintain high OLED performance whilst avoiding problems with batch-to-batch variation.

Previously, Breig *et al.* reported BT-based emissive materials with bifluorene arms and OLEDs containing the best performing material, which was capped with triphenylamine groups, showing a maximum luminance of 20,338 cd/m$^2$ and an EQE of 0.47%. In this work, we explore the performance of larger oligofluorene analogues to see how the molecular size affects device performance. Previous reports of fluorene-containing small molecules or oligomers have shown that the number of fluorene groups can influence OLED characteristics such as maximum luminance, efficiency and roll-off, and turn-on voltage.[5b,11] In this study, we show that the length of the arms attached influences the luminance, efficiency and lifetime of the OLED devices. These devices were fabricated using solution-processing to deposit the hole transport, emissive and electron transport layers, highlighting how these devices can be applied for low-energy fabrication processes.

## Experimental

### General

All reagents were purchased from commercial sources and used without further purification unless otherwise stated. Tetrahydrofuran used in reactions was obtained from an Innovative Technology Inc. Pure Solv 400-5-MD solvent purification system (activated alumina columns). $^1$H and $^{13}$C NMR spectra were recorded on AVIII 400 MHz spectrometer, at 400 and 101 MHz, respectively. Chemical shift values are presented in ppm. Low resolution mass spectrometry was carried out by matrix-assisted laser desorption/ionisation (MALDI), with dithranol used as matrix, using a Shimadzu Axima CFR spectrometer at the University of Strathclyde. Elemental analysis was carried out using an Exeter CE-440 elemental analyser.

Thermogravimetric analysis (TGA) was carried out using a Netzsch TG 209 F3 Tarsus Thermogravimetric Analyser with a nitrogen flow. Differential scanning calorimetry was run on a Netzsch DSC 214 Polyma instrument under nitrogen.

Absorption spectra were recorded using a Shimadzu UV-2600 spectrophotometer. Emission spectra and photoluminescence quantum yield (PLQY) were measured using an Edinburgh Instruments FS5 spectrofluorometer. All phosphorescence spectra were obtained from thin films deposited on a 1-inch square quartz substrate from 150 μL of a 10 mg/mL solution of the fluorescent molecule in chloroform. Spin coating was performed at 33 rps for a period of 60 s, giving a thin film of approximately 900 nm thickness.

Samples were held in a custom-made glass Dewar filled with liquid nitrogen for the duration of the study. The LED excitation wavelength was 365 nm and the spectra were measured using an Instrument Systems GmBh CAS 140 VT-151 spectrometer. The integration time for each measurement was 1 s and the results presented are the average of 5 measurements. Data was smoothed using the Savitsky-Golay filter in Origin 2020 software.

Cyclic voltammetry (CV) measurements were obtained using a CH Instruments 602E electrochemical workstation with iR compensation. The electrochemistry experiments were carried out at an analyte concentration of $10^{-4}$ M in $CH_2Cl_2$ with 0.1 M tetra-n-butylammonium hexafluorophosphate as the electrolyte and glassy carbon, platinum wire and silver wire used as the working electrode, counter electrode and quasi-reference electrode, respectively. All data is referenced to $Fc/Fc^+$ redox couple. Atomic force microscopy was carried out using a Bruker Innova microscope. All scans consisted of 512 points and 512 lines and were carried out over a scan area of $10\times10$ μm$^2$. Nanoscope Analysis 1.5 program was used for analysis of the images and calculation of the root mean square roughness (Rq).

Density functional theory (DFT) and time-dependent density functional theory (TDDFT) calculations were carried out using Gaussian 09 software,[12] version A.02. In the models, hexyl side chains were shortened to methyl groups to lessen the computational cost. Structures were first optimised and frequencies calculated using B3LYP[13] and 6-31G(d) functional and basis set, respectively, and the optimised structures were then used to simulate optical properties using TDDFT calculations with the same functional and basis set. Molecular orbitals (MO) were visualised using GaussView 5.0 software.

### Device fabrication

Substrates of pre-patterned ITO (KINTEC, 7 Ω/sq, $1.5\times1.5\times0.1$ cm$^3$ substrate dimensions) were cleaned with deionised water, acetone and isopropanol, separately, in an ultrasonic bath followed by 5 min of oxygen plasma cleaning. PEDOT:PSS (Al 4083 from Ossila) was filtered and spin-coated onto the substrates of pre-cleaned ITO and annealed at 120 °C for 20 min. These substrates were introduced into a glove box (MBRAUN). For the three compounds, solutions were prepared by using toluene with varying concentrations of 10 and 20 mg ml$^{-1}$. For all the compounds, 20 mg ml$^{-1}$ was the best solution concentration. After the deposition of the emissive layer, the films were annealed for 20 min at 40, 60 and 80 °C. After the deposition of the new compounds TPBi was spin-coated as electron transport layer (ETL) using a literature procedure,[14] and then the films were introduced into a thermal evaporation chamber for evaporation of the electrodes. An evaporation of 1 nm of LiF or 40 nm of Ca were used before the deposition of 100 nm of Al. The active area of the electrodes was $1.5\times3.5$ mm$^2$ and was deposited at a base pressure of $6\times10^{-6}$ mbar. For each set of OLED fabrication conditions, three OLEDs were tested to ensure reproducibility and the repeated results are shown in figure S25. An atomic force microscope (AFM) (Bruker, Innova) was used to determine the film thickness. *JVL* and lifetime tests were measured inside the glove box. A Keithley Semiconductor Analyser 4200 was used to bias the OLEDs and luminance measurements were performed using a Irradian Ltd. L203 photometer with a calibrated silicon photodetector with a photopic filter. These calibrations can be traced back to the National Physical Laboratory, London standards. Electrolumines-

cence spectra were measured by using an Ocean Optics USB2000+ spectrometer. External quantum efficiency was calculated by using the EL spectra and the *J–L* characteristics by considering that the light emission to be perfectly diffusive from the emission surface.[15]

### Synthesis

#### *BT-F4$_2$*

BT-(F2Br)$_2$ (0.5 g, 0.31 mmol),[16] TMS-BF-BE (0.75 g, 0.92 mmol)[7] and barium hydroxide octahydrate (0.47 g, 1.49 mmol) were added to a flask which was evacuated and purged with Ar (×3). Tetrahydrofuran (25 ml) and deionised $H_2O$ (2.5 ml) were added before the reaction mixture was degassed by bubbling with argon for 1 h. $Pd(PPh_3)_4$ (0.072 g, 0.062 mmol) was then added and the reaction mixture was stirred at reflux, under argon for 64 h. The reaction mixture was cooled and diluted with $CH_2Cl_2$ (100 ml) before being washed with deionised $H_2O$ (3×100 ml). The organic phase was then dried over $MgSO_4$, filtered and the solvent removed under reduced pressure to give the crude product. This was purified by column chromatography (silica gel, eluent – 15% $CH_2Cl_2$ in petroleum ether 40–60 °C→20% $CH_2Cl_2$ in petroleum ether 40–60 °C) followed by reprecipitation ($CH_2Cl_2$/MeOH) to give the product as a bright yellow solid. Yield = 0.85 g (93.8%). $^1$H NMR ($CDCl_3$, 400 MHz) $\delta_H$ 8.09 (d, *J* = 8.9 Hz, 2H), 8.03 (s, 2H), 7.95 (m, 4H), 7.92–7.78 (m, 12H), 7.78–7.59 (m, 26H), 7.57–7.49 (m, 4H), 2.35–1.89 (m, 32H), 1.23–1.06 (m, 96H), 0.99–0.72 (m, 80H), 0.35 (s, 18H); $^{13}$C NMR ($CDCl_3$, 101 MHz) $\delta_C$ 154.6, 152.3, 152.0, 151.93, 151.86, 151.6, 150.3, 141.6, 141.2, 141.0, 140.8, 140.72, 140.65, 140.5, 140.24, 140.19, 140.16, 140.1, 140.0, 139.1, 136.4, 133.8, 132.0, 128.4, 128.1, 127.8, 126.3, 126.2, 124.2, 121.7, 120.4, 120.1, 120.0, 119.2, 55.55, 55.50, 55.48, 55.3, 40.5, 40.3, 31.7, 31.6, 31.5, 24.1, 24.0, 23.9, 22.75, 22.71, 22.6, 14.20, 14.17, 14.16, −0.7; m/z (MALDI): 2940.05 $[M]^+$; anal. calculated for $C_{212}H_{276}N_2SSi_2$: C, 86.59, H, 9.46, N, 0.95%. Found: C, 86.96, H, 9.50, N, 1.01%. Melting point (DSC): 207.9 °C.

#### *BT-F5$_2$*

BT-(F3Br)$_2$ (0.5 g, 0.21 mmol),[17] TMS-BF-BE (0.53 g, 0.66 mmol)[7] and barium hydroxide octahydrate (0.32 g, 1.01 mmol) were added to a flask which was evacuated and purged with Ar (×3). Tetrahydrofuran (20 ml) and deionised $H_2O$ (2 ml) were added, and the reaction mixture was degassed by bubbling with argon for 1 h. $Pd(PPh_3)_4$ (0.049 g, 0.042 mmol) was added and the reaction mixture was stirred at reflux, under argon for 42 h. The reaction was then allowed to cool before being diluted with $CH_2Cl_2$ (100 ml) and washed with deionised $H_2O$ (3×100 ml). The organic phase was then dried over $MgSO_4$, filtered and the solvent was removed under reduced pressure to yield the crude product. This was purified by column chromatography (silica gel, eluent – 10% $CH_2Cl_2$ in petroleum ether 40–60 °C→20% $CH_2Cl_2$ in petroleum ether 40–60 °C) followed by reprecipitation ($CH_2Cl_2$/MeOH) to give the product as a bright yellow solid. Yield = 0.63 g (79.9%). $^1$H NMR ($CDCl_3$, 400 MHz) $\delta_H$ 8.09 (d, *J* = 8.4 Hz, 2H), 8.04 (s, 2H), 7.96 (m, 4H), 7.92–7.79 (m, 16H), 7.79–7.59 (m, 34H), 7.56–7.49 (m, 4H), 2.42–1.83 (m, 40H), 1.26–1.06 (m, 120H), 0.98–0.66 (m, 100H), 0.35 (s, 18H); $^{13}$C NMR ($CDCl_3$, 101 MHz) $\delta_C$ 154.6, 152.3, 152.0, 151.9, 151.6, 150.3, 141.6, 141.2, 141.0, 140.8, 140.71, 140.68, 140.67, 140.5, 140.23, 140.18, 140.17, 140.1, 140.0, 139.1, 136.4, 133.8, 132.0, 128.4, 128.1, 127.8, 126.3, 126.2, 124.2, 121.7, 120.4, 120.1, 120.0, 119.2, 55.54, 55.49, 55.25, 40.5, 40.3, 31.7, 31.6, 31.5, 24.1, 24.0, 23.9, 22.75, 22.71, 22.6, 14.20, 14.17, 14.15, −0.7; m/z (MALDI): 3605.98 $[M]^+$; anal. calculated for $C_{262}H_{340}N_2SSi_2$: C, 87.27, H, 9.50, N, 0.78%. Found: C, 87.52, H, 9.50, N, 0.86%. Melting point (DSC): 257.7 °C.

## Results and Discussion

### Synthesis

Compound **BT-F3$_2$** and intermediate materials and BT(F2Br)$_2$ and BT(F3Br)$_2$ were synthesised according to previously reported procedures.[17–18] In order to synthesise **BT-F4$_2$** and **BT-F5$_2$**, their respective precursors BT(F2Br)$_2$ and BT(F3Br)$_2$, were reacted with TMS-BF-BE in Suzuki-Miyaura coupling reactions (scheme 1) to give the final compounds in excellent yields of 94% and 80%, respectively. The $^1$H and $^{13}$C NMR spectra of **BT-F4$_2$** are shown in Figures S1 and S2, respectively, whilst the respective spectra for **BT-F5$_2$** are shown in Figures S3 and S4.

### Differential Scanning Calorimetry

Thermal properties such as the glass transition temperature have a strong influence on OLED device lifetime.[19] Therefore, in order to understand the influence of the oligomer size on the thermal properties, thermogravimetric analysis (TGA) and differential scanning calorimetry (DSC) scans were carried out for each of the materials. The TGA plots for **BT-F3$_2$**, **BT-F4$_2$** and **BT-F5$_2$** are shown in Figures S5, S6 and S7, respectively. The temperatures of 5% mass loss for the materials are 428 °C, 430 °C and 434 °C for **BT-F3$_2$**, **BT-F4$_2$** and **BT-F5$_2$**, respectively. The degradation temperatures are very similar with only a very small increase in stability with increasing molecular size observed.

Heat-cool-heat cycles were carried out for DSC analysis. The first heat scan was to remove any thermal history and the subsequent cooling and heating cycles are shown in Figures S8, S9 and S10 for compound **BT-F3$_2$**, **BT-F4$_2$** and **BT-F5$_2$**, respectively. There are three processes observed in the DSC scans for each material, glass transitions and melting upon heating and crystallisation upon cooling. The temperatures of these transitions are listed in Table 1. The glass transition temperature increases as the number of fluorene units in the oligomers increase. However, there is a larger effect on the melting point (Tm) and crystallisation temperatures (Tc). There is a large increase of over 80 °C in both phase transitions when comparing **BT-F4$_2$** to **BT-F3$_2$** and almost a further 50 °C increase for Tm and Tc in **BT-F5$_2$**. The oligomer size has a strong

**Table 1.** Temperatures for transitions determined by DSC and temperature of 95% mass determined by TGA.[a]

| Compound | $T_g$ [°C] | $T_m$ [°C] | $T_c$ [°C] | $T_{95\%\ mass}$ [°C] |
|---|---|---|---|---|
| **BT-F3$_2$** | 77.4 | 120.5 | 110.6 | 428 |
| **BT-F4$_2$** | 84.1 | 207.9 | 200.7 | 430 |
| **BT-F5$_2$** | 88.6 | 257.7 | 249.5 | 434 |

[a] $T_g$ = glass transition temperature, $T_m$ = melting point, $T_c$ = crystallization temperature and $T_{95\%\ mass}$ is the temperature of 5% mass loss.

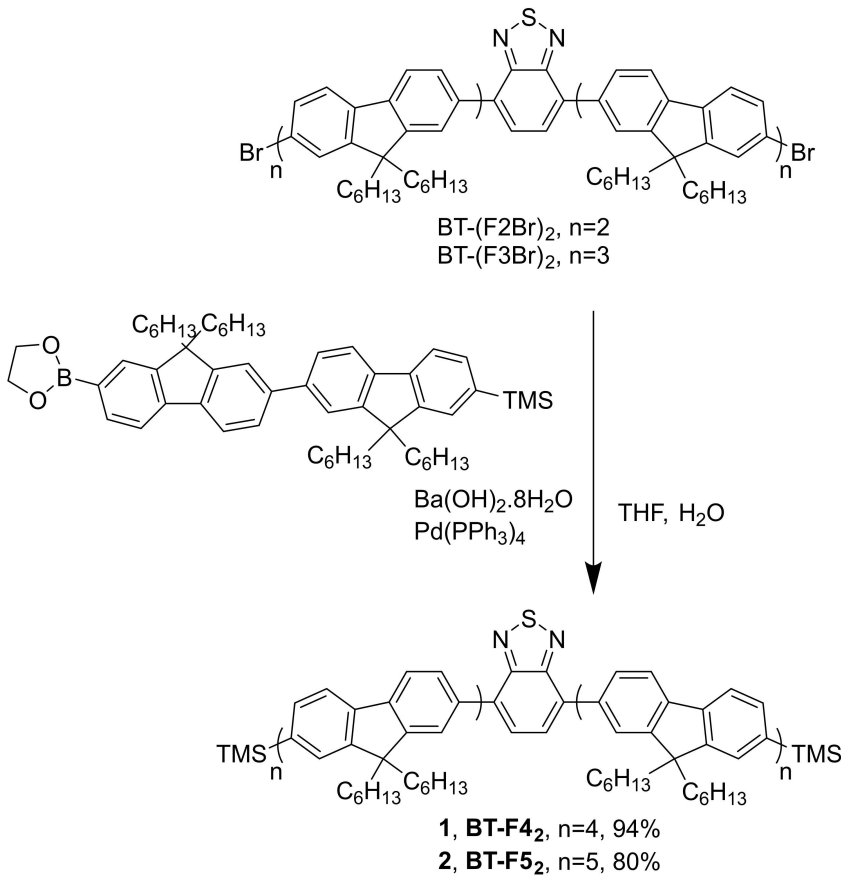


**Scheme 1.** Synthesis of **BT-F4$_2$** and **BT-F5$_2$**.

influence in thermal properties and an increase in molecular weight can improve the ability for the material to be processed at higher temperatures.

## Optical and Electrochemical Properties

UV/vis absorption and emission spectroscopy, and cyclic voltammetry were studied in order to understand the optical and electrochemical properties of the BT-based oligofluorene molecules. The data are summarised below in Table 2. The absorption and emission spectra of **BT-F3$_2$**, **BT-F4$_2$** and **BT-F5$_2$** in $CH_2Cl_2$ and thin film are shown in in Figures S11, S12 and S13, respectively. In the solution spectrum, **BT-F3$_2$** has an absorption maximum at 360 nm and a less intense peak at 423 nm. The shorter wavelength peak can be attributed to the $\pi$–$\pi^*$ transition of the oligofluorene arms and is at a similar wavelength to a previously reported terfluorene-based molecule ($\lambda_{max}$ = 353 nm).[20] The longer wavelength peak can be attributed to the transition from the conjugated backbone to

**Table 2.** Summary of optical and electrochemical properties.

| | $\lambda_{abs}$ [nm][a] | $\lambda_{em}$ [nm][a,b] | $E_{g\ opt}$ [eV][c] | $\Phi_{PL}$[d,e] | $S_1$ [eV][e,f] | $T_1$ [eV][e,g] | $E_{ox}$ [V][h] | $E_{red}$ [V][i] | HOMO [eV][j] | LUMO [eV][j] | $E_{g\ Echem}$ [eV][k] |
|---|---|---|---|---|---|---|---|---|---|---|---|
| **BT-F3$_2$** | 423, 360 (434, 358) | 569 (546) | 2.54 | 0.93 | 2.45 | 2.83 | 0.81/0.74 0.96/0.91 1.06/1.01 | −2.04/−1.60, irr | −5.6 | −3.0 | 2.6 |
| **BT-F4$_2$** | 425, 369 (433, 366) | 567 (546) | 2.54 | 0.96 | 2.46 | 2.80 | 0.69/0.63 0.83/0.78 1.10/0.96, qr | −1.96/−1.89 | −5.5 | −2.9 | 2.6 |
| **BT-F5$_2$** | 427, 372 (437, 370) | 568 (545) | 2.55 | 0.74 | 2.48 | 2.81 | 0.66/0.61 0.76/0.72 0.95/0.94 | −1.88/−1.81 | −5.4 | −3.0 | 2.4 |

[a] Peaks for thin films shown in parentheses, [b] Excited at $\lambda_{max\ abs}$; [c] $E_{g\ opt} = 1240/\lambda_{max\ abs}$; [d] Excited at 425 nm for each spectra; [e] measured in the thin film; [f] estimated from the onset of fluorescence spectra; [g] estimated from onset of phosphorescence spectra at 77 K; [h] qr = quasi-reversible; [i] irr = irreversible; [j] HOMO(LUMO) = −4.8−$E_{1/2\ ox(red)}$; [k] $E_{g\ Echem}$ = −(HOMO–LUMO).

the BT core. This has partial charge transfer character, with the reduced orbital overlap and subsequently lower transition dipole moment, explaining why this peak is less intense than the higher energy peak.[21]

The absorption spectrum of **BT-F4$_2$** in dichloromethane shows a maximum at 369 nm, with a smaller peak at 425 nm. The two peaks overlap as the molecular length increases. This is especially true for the spectrum of **BT-F5$_2$** where the BT transition appears as a shoulder at 427 nm whereas the absorption maximum for the longest molecule is 372 nm, 3 nm red-shifted from **BT-F4$_2$**. The emission spectra, excited at the $\lambda_{max}$ absorbance for each compound, are very similar for the compounds in dichloromethane solutions, with peaks of maximum emission at 569, 567 and 568 nm for **BT-F3$_2$**, **BT-F4$_2$** and **BT-F5$_2$**, respectively. The large effective Stokes shifts observed in Figures S11–S13, together with negligible self-absorption, are either due to a large change in geometry upon relaxation of the photoexcited state or by energy transfer between emissive units (oligofluorene and BT-centred).[7,22]

While there is a red shift in absorption for the thin films, there is a blue shift in the emission of the films. This is explained by the excited state structure, which varies significantly from the ground state structure, as evidenced by the large Stokes shifts. Generally, molecular structures in the excited state are more sensitive to their environment than when in the ground state. In the thin film, the environment can be considered less polar than $CH_2Cl_2$ due to the abundance of alkyl side groups, hence causing a blue shift in the emission.

The small change in wavelength for the longer wavelength absorption peaks for the oligomers can be explained using observations from time-dependent density functional theory (TDDFT) calculations of the two biggest oligomers, **BT-F4$_2$** and **BT-F5$_2$**. The calculated wavelengths of absorption for these transitions were 522.3 nm and 521.8 nm for **BT-F4$_2$** and **BT-F5$_2$**, respectively. Despite the values being red-shifted compared to experimental results, the trend is reproduced with the long wavelength peak being similar for each oligomer. This is explained by studying the molecular orbitals (MOs). For this excitation, the dominant transition in the TDDFT calculations is from the highest occupied molecular orbital (HOMO) to the lowest unoccupied molecular orbital (LUMO). These MOs are shown in Figures S18 and S19. The LUMO is localised on the benzothiadiazole core and therefore, unaffected by oligomer size. The HOMO is delocalized across much of the conjugated backbone but is most prominent over the three fluorene groups either side of the BT core. As the conjugation is increased, only a small proportion of the MO reaches the peripheral fluorenes, causing only a minimal change in the donating ability of the fluorene arms. As a result, the energy of the HOMO-LUMO transition is similar for all of the oligomers.

**BT-F3$_2$**, **BT-F4$_2$** and **BT-F5$_2$** have good solubility in toluene and this solvent was used to form spin-coated films. The absorption spectra for the three compounds in the solid state are shown in Figure 2, with a difference of only 5 nm for the maximum peak of absorption for each material: 360 nm, 365 nm and 370 nm for **BT-F3$_2$**, **BT-F4$_2$** and **BT-F5$_2$** respectively. The photoluminescence quantum yields (PLQYs) of the thin films of each of the materials were also measured and the emission plots associated with these calculations are shown in Figure S14. **BT-F3$_2$** and **BT-F4$_2$** exhibited excellent PLQYs of 0.93 and 0.96, respectively, while the PLQY for a thin film of **BT-F5$_2$** was lower at 0.74. The phosphorescence spectra of thin films were also measured at 77 K and are shown in Figures S15–S17 for **BT-F3$_2$**, **BT-F4$_2$** and **BT-F5$_2$**, respectively. The calculated triplet energies for each of the compounds were similar, showing that the number of fluorene units does not have a strong influence on this.

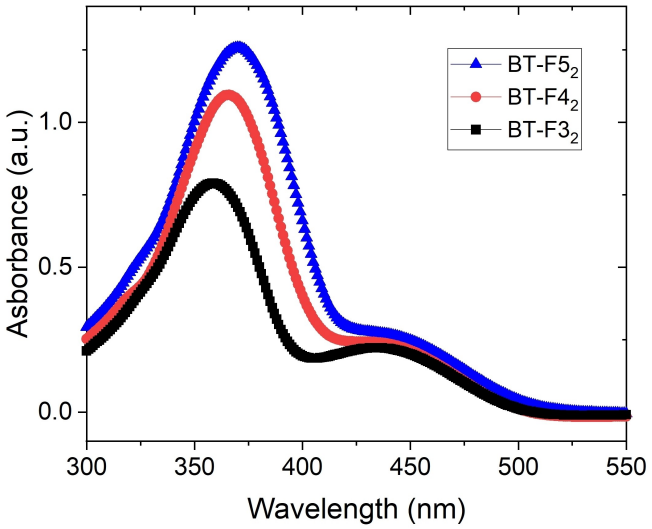


**Figure 2.** UV/Vis absorption spectra for **BT-F3$_2$**, **BT-F4$_2$** and **BT-F5$_2$** in the solid state.

Cyclic voltammetry was carried out in order to estimate the HOMO and LUMO energies from the ionisation energy and the electron affinity. All the plots are shown in Figure S20 and the data are summarised in Table 2. In general, the reduction plots are similar for each compound, with a reversible wave at ~ −1.8 to −1.9 V vs $Fc/Fc^+$, although this is quasi-reversible for **BT-F3$_2$** which shows a broad wave. Additionally, the oxidation plots are similar for all three compounds with three reversible waves occurring for each compound. The oxidation potentials generally are slightly reduced with increasing molecular length. For the first oxidation peak in each plot, this corresponds to increased HOMO energy as the molecule length increases, which is due to an increase in conjugation length. This does not affect the LUMO, which is similar for all materials, due to the localised nature of this molecular orbital, which is influenced by the electron deficient nature of benzothiadiazole.[8,17]

## OLED Devices

OLED devices were fabricated with an architecture of ITO/PEDOT:PSS/EML/TPBi/Ca (or LiF)/Al and optimised to examine the performance of **BT-F3$_2$**, **BT-F4$_2$** and **BT-F5$_2$** oligomers.

The first architecture selected was ITO/PEDOT:PSS/EML/Ca/Al to match with the LUMO and HOMO levels of the 3

compounds (approximately 2.8–3.0 eV and 5.4–5.6 eV, Figure S21). Ca/Al has a work function of 2.9 eV, which is a difference of only 0–0.1 eV with the emissive layer (EML). Therefore, the electron injection from Ca/Al to each compound should be efficient. Thermal annealing for the three materials as EMLs was optimised to improve morphology and device performance. Devices without thermal annealing and those treated at 40, 60 and 80 °C were characterised. In all the cases, annealing at 40 °C resulted in the best performance.

From the luminance and current efficiency curves for **BT-F3$_2$** devices unannealed and annealed at 40, 60 and 80 °C (Figure S22), the most significant difference is observed when the films are annealed at 80 °C. When the emissive layer is annealed at 80 °C, the turn-on voltage was increased (from 3.4 to 4 V), the luminance and the current efficiency are remarkably lower than the other 3 cases ($L_{max}$ = 8156 cd/m$^2$ and $\eta_{max}$ = 1.25 cd/A). This can be explained by the thermal properties as the glass transition temperature is below 80 °C (77.4 °C). The devices unannealed and annealed at 40 and 60 °C showed similar values of luminance (higher than 10,000 cd/m$^2$) and the same turn-on voltage. However, devices annealed at 40 °C reached a better and more stable current efficiency (2.6 cd/A).

For annealed devices of **BT-F4$_2$** at 60 and 80 °C (Figure S23), an increase in the turn-on voltage was recorded (3.6 and 3.7 V compared to 3.3 V for unannealed and 40 °C devices). Also, the current efficiency (1.7 and 1.5 cd/A, respectively) and the luminance (maximum values of 9,357 and 3,934 cd/m$^2$, respectively) were lower. The better devices were those unannealed and annealed at 40 °C, with higher maximum luminance values (7,843 and 8,511 cd/m$^2$) and current efficiencies (2.1 cd/A in both cases).

Finally, in the case of the unannealed and annealed devices with a **BT-F5$_2$** emissive layer (Figure S24), again the devices with 60 and 80 °C presented a lower performance: lower luminances (2,116 and 1,672 cd/m$^2$), higher turn on voltage (3.3 and 4.3 V compared to 3.1 V) and lower current efficiencies. The devices annealed at 40 °C presented higher luminance (4,918 *vs* 3,287 cd/m$^2$) and the same current efficiency (2.4 cd/A) as the unannealed device.

LiF/Al (workfunction *ca.* 4.1 eV) was also used as a cathode to test the influence of the cathode work function on the device performance and the devices reached luminances lower than 1,000 cd/m$^2$ due to the larger energy difference. Therefore, to improve the device performance, an electron transport layer (ETL) was added. 2,2′,2″-(1,3,5-benzinetriyl)-tris(1-phenyl-1-H-benzimidazole) (TPBi) was used as the ETL and deposited by spin coating, with the thickness for each material optimised for the multilayer architecture: ITO/PEDOT:PSS/EML/TPBi/Ca/Al. In this case TPBi also acts as a hole blocking layer due to its deep HOMO level.[23] Additionally, LiF/Al cathodes were used to improve the electron injection from the cathode to ETL (by lowering the Al work function) to compare them with those of Ca/Al. In both kinds of devices we saw an improvement in luminance, current efficiency and also the external quantum efficiency (EQE). The characteristics for the best OLED devices for both cathodes, LiF/Al and Ca/Al, are summarised in Table 3.

The devices with the interface TPBi/LiF/Al had better performance than the devices with the TPBi/Ca/Al interface. For **BT-F3$_2$**, when LiF was used instead of Ca, the luminance increased from 27,266 cd/m$^2$ to 29,499 cd/m$^2$, the current efficiency improved from 4.9 cd/A to 7.1 cd/A and $EQE_{max}$ from 1.3 % to 1.9 %. Also, the turn on voltage was improved from 3.1 V to 2.8 V.

For **BT-F4$_2$**, a large improvement of the $EQE_{max}$ can be seen when LiF is used instead Ca, doubling from 1.1 % to 2.2 %. Also, a slight improvement in the maximum luminance (26,701 cd/m$^2$ to 27,274 cd/m$^2$) was observed and a significant increase in the current efficiency (4.4 cd/A to 8.3 cd/A) because of the lowered current density.

Finally for **BT-F5$_2$** the luminance remains similar when changing from Ca to LiF (20,756 cd/m$^2$ to 20,496 cd/m$^2$), but the current efficiency (6.2 cd/A to 7.4 cd/A) and the $EQE_{max}$ (1.6 % to 2 %) increase. The curves of luminances and current efficiencies *vs* voltage for the best OLED device of each molecule are shown in Figure 3. In all cases the efficiency of the devices was improved when LiF/Al cathode was used, probably because the work function level of the Al is closer to the LUMO level of the ETL compared with the Ca/Al case.

The maximum peak of electroluminescence is similar for each compound at 543 nm for **BT-F3$_2$** and 541 nm for **BT-F4$_2$** and **BT-F5$_2$** (Figure 4). Also, the chromaticity coordinates (x,y) in the Commission Internationale d'Eclairage (CIE) 1931 colour space chromaticity diagram were calculated as (0.39,0.60) for the three compounds. Interestingly this is blue-shifted compared to the previously reported analogue green 1 (or **BT-F2$_2$**), which has bifluorene arms and which exhibited a peak EL at 556 nm.[16] Also, the EL peaks are blue-shifted with respect to the photoluminescence spectra. This suggests that the emission of these molecules has a degree of sensitivity to the environment. This would be consistent with the partial charge

**Table 3.** Performance of the best OLED devices using the oligomers **BT-F3$_2$**, **BT-F4$_2$** and **BT-F5$_2$** as EML, TPBi as ETL, Ca/Al and LiF/Al as cathodes.[a]

| Molecule (EML) | ETL/cathode interface | $V_{on}$ [V] | $L_{max}$ [cd/m$^2$] | $\eta_{Lmax}$ [cd/A] | $\eta_{max}$ [cd/A] | $L_{\eta max}$ [cd/m$^2$] | $EQE_{max}$ [%] |
|---|---|---|---|---|---|---|---|
| **BT-F3$_2$** | TPBi(50 nm)/Ca(40 nm)/Al(100 nm) | 2.8 | 27,266 | 2.6 | 4.9 | 364 | 1.3 |
| | TPBi(55 nm)/LiF(1 nm)/Al(100 nm) | 3.1 | 29,499 | 3.8 | 7.1 | 190 | 1.9 |
| **BT-F4$_2$** | TPBi(55 nm)/Ca(40 nm)/Al(100 nm) | 3 | 26,701 | 2.3 | 4.4 | 912 | 1.1 |
| | TPBi(55 nm)/LiF(1 nm)/Al(100 nm) | 3.1 | 27,274 | 3.4 | 8.3 | 265 | 2.2 |
| **BT-F5$_2$** | TPBi(55 nm)/Ca(40 nm)/Al(100 nm) | 3 | 20,756 | 2 | 6.2 | 488 | 1.6 |
| | TPBi(55 nm)/LiF(1 nm)/Al(100 nm) | 3 | 20,496 | 2.7 | 7.4 | 364 | 2.0 |

[a] $V_{on}$ = turn on voltage at 1 cd/m$^2$, $L_{max}$ = maximum luminance, $\eta_{Lmax}$ = current efficiency at maximum luminance, $\eta_{max}$ = maximum current efficiency, $L_{\eta max}$ = Luminance at maximum current efficiency.

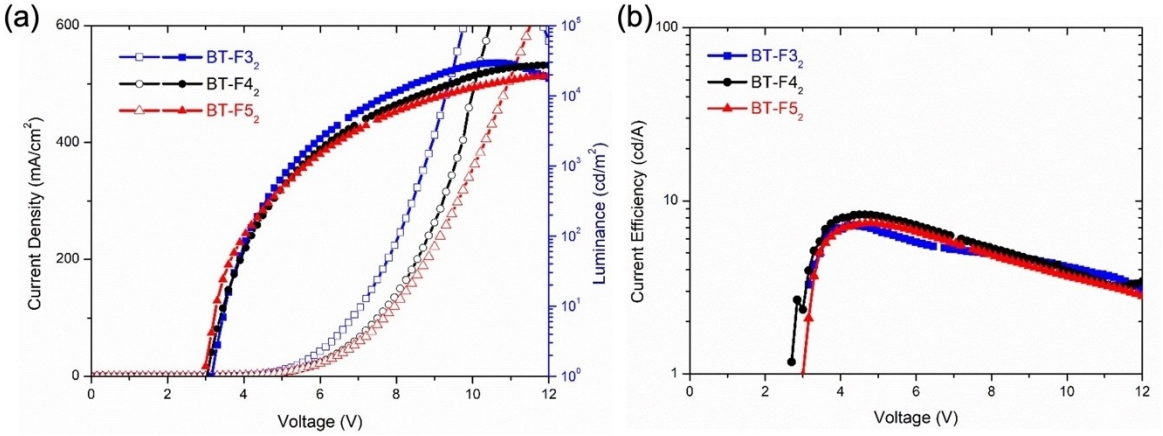


**Figure 3.** a) J–V–L curves, b) current efficiency for the OLED devices with architecture ITO/PEDOT:PSS/Molecule/TPBi/LiF/Al for **BT-F3$_2$**, **BT-F4$_2$** and **BT-F5$_2$**.

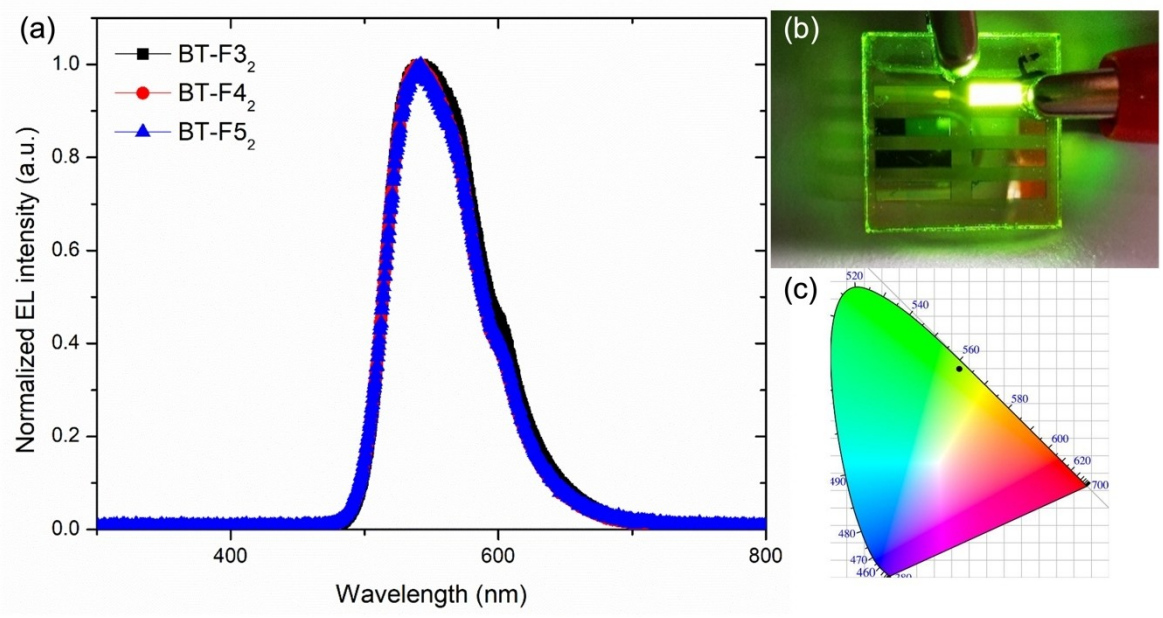


**Figure 4.** (a) Electroluminescence (EL) spectra of **BT-F3$_2$**, **BT-F4$_2$** and **BT-F5$_2$**; (b) photograph of one OLED device based on **BT-F4$_2$**; and (c) the chromaticity coordinates (0.39,0.60).

transfer character of the transition. As mentioned previously, the LUMO of each molecule is expected to be localised around the benzothiadiazole core. According to calculations on **BT-F4$_2$** and **BT-F5$_2$** and previously reported calculations on smaller analogues, the HOMO would also be predicted to be delocalised across the entire molecule.[17] Therefore, as the molecular length is increased, the spatial overlap between the HOMO and LUMO is reduced, explaining why the emission of larger BT-oligofluorene molecules is influenced more by its environment than the smaller analogues.

The film topographies of the emissive layers were studied using atomic force microscopy and are shown in Figure 5. The surface of **BT-F3$_2$** shows large, inter-connected domains, which suggests a degree of aggregation in the film. In contrast, the topography of **BT-F4$_2$** thin film is largely featureless and more homogeneous across much of the surface but the large, smooth hills and troughs contribute to a larger roughness than observed for the other two materials. The thin film of **BT-F5$_2$** shows numerous small domains of mostly uniform height distribution and many small gaps in between. Although all of the films do not have a large roughness, it is expected that the smooth topography of **BT-F4$_2$** contributes to the improved device performance.

The lifetime of the devices was also measured by monitoring the degradation in luminance over 2 hours (Figure S26) and modelled using the stretched exponential decay (SED) model, with these plots shown in Figure 6. A constant current of 20 mA/cm$^2$ was applied and the luminance was measured each minute for a few hours. Devices with a Ca/Al cathode showed a significant stability for luminance compared with those that used LiF/Al. From the experimental data for the devices with a Ca/Al cathode, it was found that the luminance of the devices

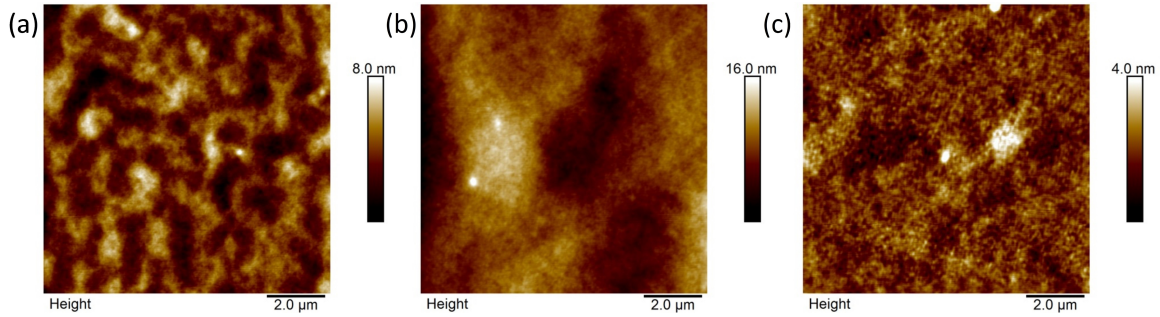


**Figure 5.** Atomic force microscopy images for films of (a) **BT-F3$_2$** (Rq = 1.13 nm), (b) **BT-F4$_2$** (Rq = 2.20 nm) and (c) **BT-F5$_2$** (Rq = 0.48 nm). Scan area = 10 × 10 μm.

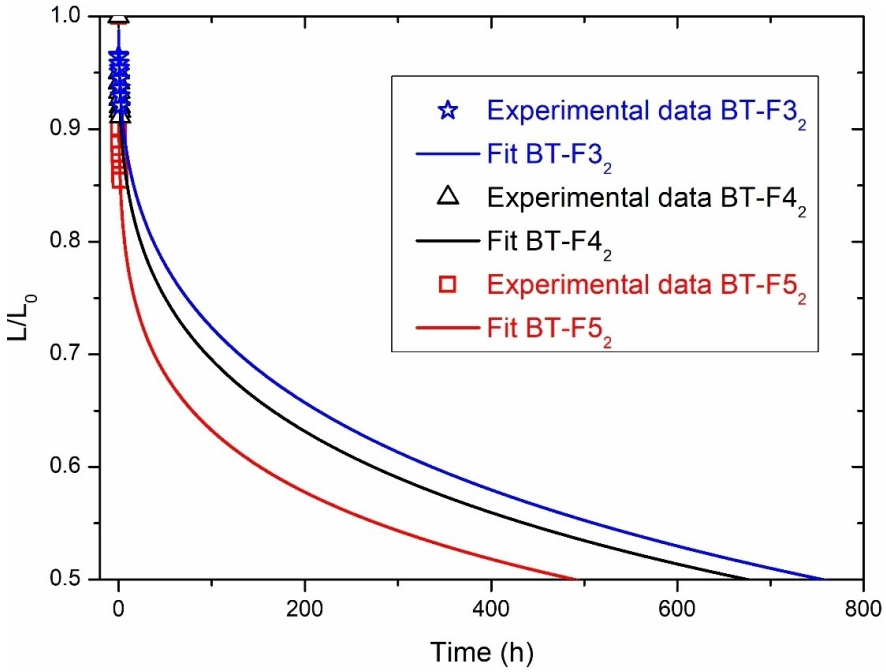


**Figure 6.** Operational lifetime (LT50) for OLED devices based on **BT-F3$_2$**($L_0$ = 948 cd/m$^2$), **BT-F4$_2$**($L_0$ = 868 cd/m$^2$) and **BT-F5$_2$**($L_0$ = 913 cd/m$^2$). Experimental data and fit by using SED model are shown.

decayed 50% (LT50) after 29,398 min (490 h) for **BT-F5$_2$**, 40,533 min (675 h) for **BT-F4$_2$** and 45,368 min (756 h) for **BT-F3$_2$**. As we have the same interfaces (ITO/PEDOT:PSS and TPBi/Ca/Al) in the three devices, it can be seen from the LT50 values that the length of the molecule has a remarkable influence in the lifetime of the devices and that at a longer length a lower lifetime is reached. LT50 for **BT-F3$_2$** was 12% higher than **BT-F4$_2$** and 54% higher than **BT-F5$_2$**. This could be explained by the fact that at a bigger length of the molecule, a higher probability exists that energy is spent by de-excitation through vibrational relaxation,[24] causing the oligomer to be heated. This temperature can induce a faster degradation of device performance. This is evident when **BT-F3$_2$** is annealed beyond its glass transition temperature for example. Therefore, we believe that there is a balance to be struck when studying the effect of molecular size of the emissive material on device lifetime. In this case, we believe that the increased Joule heating in the larger size molecules is more detrimental to device lifetime than a slightly lower glass transition temperature. This results in **BT-F3$_2$** having the longest device lifetime and highlights that modifying the glass transition temperature by increasing the molecular weight of the oligomer doesn't always result in improved lifetime.

## Conclusions

We have studied three benzothiadiazole-containing oligofluorenes for their suitability as emissive materials in OLED devices. As monodisperse, single molecules, the emissive material can avoid problems associated with batch-to-batch variation in polymers. Additionally, these were able to be applied in a fabrication process that allowed for the deposition of three layers by solution processing (hole transport, emissive and

electron transport layers), highlighting the potential for such devices to be made using low-cost, low-energy processes compared to vacuum deposited devices.

Whilst the molecular length (or number of fluorene units) had a small influence on the photophysical properties of the materials, there was a notable effect on the OLED performance. **BT-F4$_2$** showed the highest EQE$_{max}$ for the devices studied, at 2.2%, which is also significantly higher than for smaller analogues previously studied.[16] However, although **BT-F3$_2$** showed the lowest EQE$_{max}$ of the optimal devices using the different oligomer emissive layers, it showed the longest device lifetime, with the trend showing that device lifetime shortened with increased oligomer size. We therefore highlight that although larger oligomers can increase the glass transition temperature, which is generally desirable for increasing device lifetime, the increased heating effect associated with the larger molecule size has a larger influence on device lifetime in this case. Therefore, a balance is required when considering increasing oligomer size to improve both OLED efficiency and lifetime.

## Acknowledgements

*J. C. and P. J. S. thank EPSRC for funding (EP/P02744X/2). L. A. L. H. thanks CONACyT for his scholarship grant. The authors thank the European Union for funding the MSCA-RISE project, MEGA (grant agreement 823720). We thank Pat Keating (University of Strathclyde) for MALDI measurements. Supporting raw data for the manuscript can be accessed at the following address: https://doi.org/10.5525/gla.researchdata.1372.*

## Conflict of Interest

The authors declare no conflict of interest.

## Data Availability Statement

The data that support the findings of this study are openly available in University of Glasgow at https://doi.org/10.5525/gla.researchdata.1372.

**Keywords:** conjugation · fluorene · organic light-emitting diodes · photophysics · semiconductors

[1] Y.-J. Luo, Z.-Y. Lu, Y. Huang, *Chin. Chem. Lett.* **2016**, *27*, 1223–1230.
[2] a) Y. Youn, D. Yoo, H. Song, Y. Kang, K. Y. Kim, S. H. Jeon, Y. Cho, K. Chae, S. Han, *J. Mater. Chem. C* **2018**, *6*, 1015–1022; b) V. N. Hamanaka, E. Salsberg, F. J. Fonseca, H. Aziz, *Org. Electron.* **2020**, *78*, 105509.
[3] a) Q. Wei, Z. Ge, B. Voit, *Macromol. Rapid Commun.* **2019**, *40*, 1800570; b) S. M. Raupp, L. Merklein, M. Pathak, P. Scharfer, W. Schabel, *Chem. Eng. Sci.* **2017**, *160*, 113–120.
[4] a) L. Merklein, D. Daume, F. Braig, S. Schlisske, T. Rödlmeier, M. Mink, D. Kourkoulos, B. Ulber, M. Di Biase, K. Meerholz, G. Hernandez-Sosa, U. Lemmer, H. M. Sauer, E. Dörsam, P. Scharfer, W. Schabel, *Colloids Interfaces* **2019**, *3*, 32; b) L. Duan, L. Hou, T.-W. Lee, J. Qiao, D. Zhang, G. Dong, L. Wang, Y. Qiu, *J. Mater. Chem.* **2010**, *20*, 6392–6407.
[5] a) I. Bala, R. A. K. Yadav, M. Devi, J. De, N. Singh, K. Kailasam, J. Jayakumar, J.-H. Jou, C.-H. Cheng, S. K. Pal, *J. Mater. Chem. C* **2020**, *8*, 17009–17015; b) V. H. K. Fell, N. J. Findlay, B. Breig, C. Forbes, A. R. Inigo, J. Cameron, A. L. Kanibolotsky, P. J. Skabara, *J. Mater. Chem. C* **2019**, *7*, 3934–3944.
[6] Y. Wang, T. Michinobu, *J. Mater. Chem. C* **2016**, *4*, 6200–6214.
[7] C. R. Belton, A. L. Kanibolotsky, J. Kirkpatrick, C. Orofino, S. E. T. Elmasly, P. N. Stavrinou, P. J. Skabara, D. D. C. Bradley, *Adv. Funct. Mater.* **2013**, *23*, 2792–2804.
[8] J. Cornil, I. Gueli, A. Dkhissi, J. C. Sancho-Garcia, E. Hennebicq, J. P. Calbert, V. Lemaur, D. Beljonne, J. L. Brédas, *J. Chem. Phys.* **2003**, *118*, 6615–6623.
[9] M. T. B. Edmund, P. Woo, M. Inbasekaranm, W. Wu, *US Patent 6309763*, **1998**.
[10] B. R. Lee, E. D. Jung, J. S. Park, Y. S. Nam, S. H. Min, B.-S. Kim, K.-M. Lee, J.-R. Jeong, R. H. Friend, J.-S. Kim, S. O. Kim, M. H. Song, *Nat. Commun.* **2014**, *5*, 4840.
[11] C.-G. Zhen, Z.-K. Chen, Q.-D. Liu, Y.-F. Dai, R. Y. C. Shin, S.-Y. Chang, J. Kieffer, *Adv. Mater.* **2009**, *21*, 2425–2429.
[12] M. J. Frisch, G. Trucks, H. B. schlegel, G. E. Scuseria, M. A. Robb, Gaussian 09 version A.02, **2009**.
[13] a) A. D. Becke, *Phys. Rev. A* **1988**, *38*, 3098–3100; b) C. Lee, W. Yang, R. G. Parr, *Phys. Rev. B* **1988**, *37*, 785–789.
[14] N. Aizawa, Y.-J. Pu, M. Watanabe, T. Chiba, K. Ideta, N. Toyota, M. Igarashi, Y. Suzuri, H. Sasabe, J. Kido, *Nat. Commun.* **2014**, *5*, 5756.
[15] S. Okamoto, K. Tanaka, Y. Izumi, H. Adachi, T. Yamaji, T. Suzuki, *Jpn. J. Appl. Phys.* **2001**, *40*, L783–L784.
[16] N. J. Findlay, B. Breig, C. Forbes, A. R. Inigo, A. L. Kanibolotsky, P. J. Skabara, *J. Mater. Chem. C* **2016**, *4*, 3774–3780.
[17] J. E. Greenwald, J. Cameron, N. J. Findlay, T. Fu, S. Gunasekaran, P. J. Skabara, L. Venkataraman, *Nat. Nanotechnol.* **2021**, *16*, 313–317.
[18] N. J. Findlay, B. Breig, C. Forbes, A. R. Inigo, A. L. Kanibolotsky, P. J. Skabara, *J. Mater. Chem. C* **2016**, *4*, 3774–3780.
[19] J. A. McEwan, A. J. Clulow, A. Nelson, N. R. Yepuri, P. L. Burn, I. R. Gentle, *ACS Appl. Mater. Interfaces* **2017**, *9*, 14153–14161.
[20] L. Zhu, C. Zhong, Z. Liu, C. Yang, J. Qin, *Chem. Commun.* **2010**, *46*, 6666–6668.
[21] R. J. Magyar, S. Tretiak, *J. Chem. Theory Comput.* **2007**, *3*, 976–987.
[22] A. L. Kanibolotsky, N. Laurand, M. D. Dawson, G. A. Turnbull, I. D. W. Samuel, P. J. Skabara, *Acc. Chem. Res.* **2019**, *52*, 1665–1674.
[23] S.-C. Lo, N. A. H. Male, J. P. J. Markham, S. W. Magennis, P. L. Burn, O. V. Salata, I. D. W. Samuel, *Adv. Mater.* **2002**, *14*, 975–979.
[24] M. Zhu, C. Yang, *Chem. Soc. Rev.* **2013**, *42*, 4963–4976.

Manuscript received: September 20, 2022
Revised manuscript received: November 9, 2022
Accepted manuscript online: November 11, 2022
Version of record online: December 7, 2022